SCIENCE CHINA
Earth Sciences

• RESEARCH PAPER •

November 2012 Vol.55 No.11: 1855–1871
doi: 10.1007/s11430-012-4421-4

Modulation of land-sea thermal contrast on the energy source and sink of tropical cyclone activity and its annual cycle

YING Ming[1], WU GuoXiong[2*], LIU YiMin[2] & SUN ShuQing[2]

[1] *Shanghai Typhoon Institute of China Meteorological Administration, Shanghai 200030, China;*
[2] *State Key Laboratory of Numerical Modeling for Atmospheric Sciences and Geophysical Fluid Dynamics, Institute of Atmospheric Physics, Chinese Academy of Sciences, Beijing 100029, China*

Received September 30, 2011; accepted February 23, 2012; published online June 16, 2012

In general, the tropical cyclone (TC) activity is considered to be influenced by the heat content of underlying ocean, vertical shear of horizontal wind, vorticity in the low troposphere, moisture in the troposphere, and favorable condition for deep convection development. However, these factors by nature merely present the internal factors of either atmosphere or ocean which influence the TC activity. In fact, the energy budget of the Earth system and its variation, modulated by the land–sea thermal contrast, are the intrinsic reasons responsible for the variation of TC activity. Here we investigate the modulation of diabatic heating distribution associated with the land–sea thermal contrast on the distribution of TC activity energy source and sink as well as the seasonality. An accumulated energy increment index (AEI) is defined using the TC best track data, and the energy sources and sinks of TC activity are then diagnosed effectively and practically according to the distribution of AEI. Results show that the thermal contrast of land and ocean is the primary reason for asymmetric distribution of TC activity about the Equator as well as the zonally asymmetric distribution of TC activity. The energy sources of TC activity are dominated by condensation heating of deep convection or double-dominant heating, which includes the condensation heating and cooling of longwave radiation (LO), while the sink areas are dominated by LO. The large scale diabatic heating associated with land-sea thermal contrast results in more favorable conditions for TC activity over the west part of oceans than those over the east parts. Moreover, the intensity of interaction of different diabatic heating over the west and east parts of ocean is also affected by the zonal scale of the oceans, which induces the difference of TC activity over the western North Pacific (WNP) and North Atlantic (ATL). The favorable westerlies and anticyclonic vertical shear associated with the tropical zonally asymmetric diabatic heating also contribute to the most intense TC activity over the WNP. The variation of large scale diabatic heating modulates the annual cycle of TC energy sources and sinks. In particular, the annual cycle over the WNP is the most typical one among the three basins (the WNP, the south Indian Ocean, and western South Pacific) that are characterized by the meridional shift of the energy sources and sinks. However, sources over the eastern North Pacific tend to extend westward and withdraw eastward associated with the variation of LO, while over the ATL, sources always merge from small pieces into a big one as the different diabatic heating over its west and east parts interacts with each other. Over the boreal Indian Ocean, the subcontinental scale land-sea heating contrast modifies the large scale circulation, and consequently contributes to the bimodal annual cycle of TC activity. In summary, TC activities are closely related to the interaction among various components of the climate system more than the atmosphere and ocean.

land-sea thermal contrast, tropical cyclone, energy sources and sinks, seasonality

Citation: Ying M, Wu G X, Liu Y M, et al. Modulation of land-sea thermal contrast on the energy source and sink of tropical cyclone activity and its annual cycle. Sci China Earth Sci, 2012, 55: 1855–1871, doi: 10.1007/s11430-012-4421-4

*Corresponding author (email: gxwu@lasg.iap.ac.cn)

The land-sea thermal contrast is one of the important factors for formation of the current general circulation. The monsoon circulation is the most typical response of the atmosphere to this thermal contrast [1] as the gradient of air pressure induced by the land-sea thermal contrast is one of the driving mechanisms of the monsoon circulation [2, 3]. Wu and Liu [4] and Liu et al. [5] found that the summertime diabatic heating over the subtropical continents and their adjacent oceans are organized as quadruplet patterns called LOSECOD, that is, strong longwave radiative cooling (LO) over the east part of the ocean, sensible heating (SE) and condensation heating (CO) dominant over the western and eastern portions of the continent, respectively, and the double dominant heating (D), with LO prevailing CO, over the western part of the ocean. The LOSECOD heating quadruplet is always accompanied with a distinct circulation pattern with an anticyclonic circulation over the continent in the upper troposphere and cyclonic circulations, over the adjacent oceans, on both the western and eastern sides of the anticyclone, or vice versa near the surface. This interprets the zonally asymmetrical characteristics of subtropical circulation. Wu et al. [6] further demonstrated how the air-sea interaction is modulated by the distribution of continents and oceans and the mechanism of self-organization of LOSECOD. Keep in mind that the continent is colder in winter and hotter in summer than the ocean, the land-sea thermal contrast enhanced the upward sensible heat flux over the western part of the ocean in wintertime, and *vice versa* in summertime. The monsoon circulation is induced by and feedbacks on the distribution of diabatic heating. On the other hand, adaption to the LO-SE heating over the western part of continent and its adjacent ocean on the western side, the anomalous sensible heat flux over the eastern part of ocean is from the atmosphere to the ocean in the wintertime and vice versa in the summertime. Meanwhile, the cold coastal northerlies are induced by the synchronous forcing of LO and SE. The land-sea contrasts of the thermal forcing become even larger because of the offshore upwelling induced by the coastal northerlies and the enhanced sensible heat flux induced by the thermal discrepancies between the cold air flow and the land surface [6]. Moreover, the modulation of land-sea thermal contrast on air-sea interaction is also obvious over the South Asia and may have important influences on both development and translation of the monsoon onset vortex in the Bay of Bengal [7]. Therefore, the land-sea thermal contrast is one of the essential factors of the climate variabilities, and it has influences not only on the climate regime but also on the interactions among different components of the climate system.

On seasonal scale, the frequency of tropical cyclone (TC) is closely related to the ocean thermal energy, low level vorticity, vertical shear, relative humidity, and favorable conditions of convection [8]. These physical conditions were the footstone of researches not only on TC climate since 1970s, but also on climate change of TC activity since the global warming became a hot topic [9]. Accordingly, with the growing understanding on the climatology of TC activity, various phenomena have different influences on the variabilities of TC activity on different time scales, such as the tropical circulation associated the El Niño and South Oscillation (ENSO) [10–13], the Intertropical Convergence Zone (ITCZ), monsoon trough and the cold surges from another hemisphere [14–21]. However, there are obvious discrepancies of TC activity in different ocean basins, and the discrepancies were found not only in the geographic distribution, but also in the annual circle of TC activity [22]. What causes the discrepancies among different ocean basins, and why are the physical conditions so different from basin to basin? We supposed that the distribution of the continents and oceans may be an essential factor and the reasons are as follows. First, adapted to the LOSECOD heating quadruplet, anomalous anticyclonic (cyclonic) circulation is forced in the upper (low) troposphere [4], which are favorable conditions for TC activity [8]. Second, with effects of both the boundary of landmass and the wind stress, the temperatures of the western part of the ocean are usually higher than the eastern part [23, 24]. This indicates zonally asymmetric distribution of ocean thermal energy. Third, the air-sea interactions are also modulated by the thermal contrast [6]. The three aspects suggest that the physical factors of TC activity are also influenced by the distribution of continents and oceans. Moreover, TC activities are resulted from the requirements of energy redistribution of the Earth system [25], and in turn are also related to variations of the external forcing on the system. The distribution of continents and oceans modifies the balance of Earth system's energy and modulates the process of energy redistribution. Hence, the land-sea thermal contrast and its associated diabatic heating patterns construct the background of TC activity. Investigation on how the thermal contrast affects the TC activity may be helpful for understanding TC activity on various time scales. In this study, we restrict ourselves to the issue of the climatological geographic distribution of TC activity and its associated seasonality and the influences of the thermal contrast on them.

TC activity is a phenomenon with obvious seasonality. The characteristics of its seasonality are quite different over different ocean basins, with a single peak annual cycle in some basins and a bimodal annual cycle in other basins [22]. Different from the variabilities on intraseasonal and interannual scales [26, 27], the characteristics of the annual cycle of TC activity usually draw insufficient attentions. However, the variations of the beginning and duration of TC's active season as well as the amplitudes of its annual cycle have their own characteristics [28, 29] and relationship with both the intraseasonal and interannual variabilities.

Although the role of SST is dominant in the energy budget of individual TC [30, 31], it may be inappropriate to emphasize the absolute role of SST in determining TC activity with less consideration on TCs' feedback on the environment, such as studies based on thermodynamics of mature TC [32, 33]. In fact, some numerical studies on the influences of TCs on the ocean suggested that the feedback may be significant [34–36], which indicates the two-way relationship between the environmental conditions and TC activity. Therefore, inferences on the trends of TC activity only from the large scale environmental conditions may not be sufficient and the trends may include bias. In view of this, it is helpful to investigate the TC activity in the framework of interactive multi-components of the climate system. This is the reason why the influences of land-sea thermal contrast are discussed in this study.

To link the TC activity with the variabilities of climate system, an appropriate metrics beyond the frequency is necessary. Gray et al. [37] proposed the Hurricane Destruction Potential (HDP), and Bell et al. [38] used a similar parameter, called the Accumulated Cyclone Energy (ACE):

$$\mathrm{ACE} = 10^{-4}\sum_{0}^{N}\sum_{0}^{T}V_{\max}^{2}, \tag{1}$$

where $V_{\max}$ is the maximum sustained wind speed (MSW), T is the life span of TC (in unit of total times of the best track), and N is TC number. Based on the ACE, Kwon et al. [39] proposed the Normalized Typhoon Activity (NTA) index. All of the three indices are defined as accumulated square of the MSW in TC life span. The Power Dissipation Index (PDI), according to the thermodynamics of mature TCs [30, 31], is also defined in the same way, that is, based on the integration of cube of MSW. The four indices are, in their nature, functions of TC frequency, life span and intensity, and can be represented by a common formula following Wu et al. [40]:

$$\mathrm{SAI} = \sum_{0}^{N}\sum_{0}^{T}aV_{\max}^{m}, \tag{2}$$

where m is the power and a is a constant. According to formula (2), SAI has advantages in describing the intensity of TC activity, and its capability in describing seasonality of TC activity is similar to the frequency of occurrence. Actually, SAI is the frequency of occurrence when m=0 and a=1. Indices like SAI are useful for discussing the influences of large scale environment on TC activities rather than two-way interactions between them in the context of energy redistribution of the climate system. For instance, except for the differences in magnitude of values, indices like SAI over the ocean where TCs usually obtain energies are not different from the land area where TCs usually lose energies. In this paper, we try to propose a new index, the accumulated energy increment (AEI), to address this issue.

1 Data and methodology

1.1 Data and analysis procedures

The global TC best track data for period of 1951–2008 are obtained from the International Best Track Archive for Climate Stewardship (IBTrACS, available from http://www.ncdc.noaa.gov/oa/ibtracs/) [41]. The tropical depression (TD) stage (MSW < 17.2 m s^{-1}) is excluded since there were large discrepancies in TD analysis among different agencies [42]. The lifespan of individual TC is defined as starting from the first time TC reached the strength of tropical storm (TS, MSW ⩾ 17.2 m s^{-1}) and the last time TC's intensity dropped below TS. Both the AEI and ACE [38] were calculated based on the lifespan.

The diabatic heating in atmosphere is an important forcing of general circulation. Using the National Center for Atmospheric Research (NCEP) Reanalysis I data [43], the apparent heat source Q_1 and apparent moisture sink Q_2 [44, 45] are calculated from

$$Q_1 = c_p\left[\frac{\partial T}{\partial t} + \boldsymbol{V}\cdot\nabla T + \left(\frac{p}{p_0}\right)^{\kappa}\omega\frac{\partial\theta}{\partial p}\right],$$

$$Q_2 = -L\left(\frac{\partial q}{\partial t} + \boldsymbol{V}\cdot\nabla q + \omega\frac{\partial q}{\partial p}\right),$$

where T is the temperature, θ the potential temperature, q the mixing ratio of water vapor, $\boldsymbol{V}$ the horizontal velocity, ω the vertical p-velocity, p the pressure, L the latent heat of condensation, p_0 = 1000 hPa. In the equation $\kappa = R/c_p$, R and c_p are the gas constant and the specific heat at constant pressure of dry air, respectively. The values of Q_1 are determined by the term of radiative cooling, the net condensation of water vapor, and vertical transport of sensible heating by the small scale eddies, whereas the values of Q_2 are determined by net condensation of water vapor and vertical transport of water vapor by the small scale eddies. Integrating Q_1 and Q_2 from the tropopause pressure to the surface pressure, we have

$$\langle Q_1\rangle = \langle Q_{\mathrm{R}}\rangle + LP + S,$$

$$\langle Q_2\rangle = L(P - E),$$

where Q_{R} is the radiative heating rate, and S, P and E are the sensible heat flux, the precipitation rate and the evaporation rate, respectively. The characteristics of the diabatic heating can be inferred from the patterns of Q_1 and Q_2 [44, 46]. Moreover, we also used the diabatic heating rate derived from the monthly NCEP reanalysis data on 192×94 Gaussian grid and 28 levels of vertical terrain following sigma coordinate [43]. The same data had been used by Wu and Liu [4] and Liu et al. [5].

1.2 Definition of the AEI index

According to the ideal model of mature TC, the TC keeps a dynamic balance between the heat input and dissipation of kinetic energy in the atmospheric boundary layer, and its intensity change is closely related to the energy budget [30, 31, 47]. In other words, the TC intensity is an indicator of its energy change. The TC is intensified by excess of energy and weakened because of deficit of energy. The TC's energy is a function of its size and the radial profile of its wind. However, both are deficient in observations with only a few estimations in some area [48, 49]. Mallen et al. [50] suggested that the radial profiles of wind for different TC cases had similar geometric shapes when they were normalized by the MSW [50]. Further analysis (Appendix A) indicates that the contribution of the variation of TC size to the energy changes can be explained partly by the changes of MSW. Therefore, the accumulated energy increment (AEI) is defined as

$$\mathrm{AEI}_{(i,j)} = \frac{1}{K}\sum_{k=1}^{K}\sum_{n=1}^{N_k}\int_{t_1(n)}^{t_2(n)}\frac{\partial V_{kn}^2}{\partial \tau}\mathrm{d}t, \tag{3}$$

where τ is the time interval of the observations, which set to 6 h according to the temporal resolution of the best track data, $t\in[t_1(n), t_2(n)]$ is the temporal period that the nth TC stays in the grid (i, j), N_k is the total number of TCs passing the grid during the target season (or month) of the kth year, and K is the total years. According to the relationship between TC's intensity and its energy budget [30, 31], the formula (3) indicates that, for individual TC staying within the grid (i, j), the positive value of AEI means TC is intensified as net energy input while the negative value of AEI means TC is weakened as net energy loss. Consequentially, the AEI for all TCs occurring in the target season (or month) demonstrates the climatic energy sources (with net energy input) and sinks (with net energy loss) of TC activity in the season (or month). In other words, the zero value of AEI draws the line between the energy sources and sinks. With the definition of TC's lifespan in section 2.1, when the grid (i, j) is expanded to the whole basin, AEI must be zero with ignoring a few cross basin cases. This indicates the energy balance of TC activity within a basin.

Specifically, Figure 1 shows the climatology of both AEI and ACE of TC activity. As shown in Figure 1(a), the AEI is positive over most part of the tropical oceans but negative over extratropical oceans and the land area, including tropical islands near the 120°E, Central America, and West Indies. The pattern of AEI matches well with the knowledge on TC's energy sources and sinks. That is, TCs usually obtain energy from the warm tropical oceans, and lose energy either over the extratropical regions or land area because of insufficient energy supply or enhanced friction damping of the land surface, respectively. In contrast to the AEI pattern, the ACE index, as the combination of the frequency, intensity and lifespan, can only demonstrate a relative intensity of TC activity (Figure 1(b)). Therefore, although the AEI and the indices like SAI are all defined by the best track data, the AEI has its advantages in linking the TC activity with the energy redistribution of the climate system rather than describing the TC activity as collection of weather events.

2 The energy sources and sinks of TC activity

2.1 Climatology

As shown in Figure 1(a), the largest positive AEI values are over the western Pacific region to the west of 160°E and the eastern Pacific region to the east of 120°W, respectively. Both regions are very close to the warm pools in either the western or the eastern Pacific. This indicates that the zonally asymmetric pattern of ocean thermal condition has influences on the distribution of energy sources of TC activity.

On the other hand, both the negative and positive AEI regions are zonally asymmetric and dissymmetric about the Equator, with more intense AEI in the north hemisphere than in the south hemisphere. Amongst global basins with TCs, the energy sources and sinks of TC activity are both limited to the tropics only over the basins of boreal Indian Ocean (BIO) and eastern North Pacific (ENP). Meanwhile,

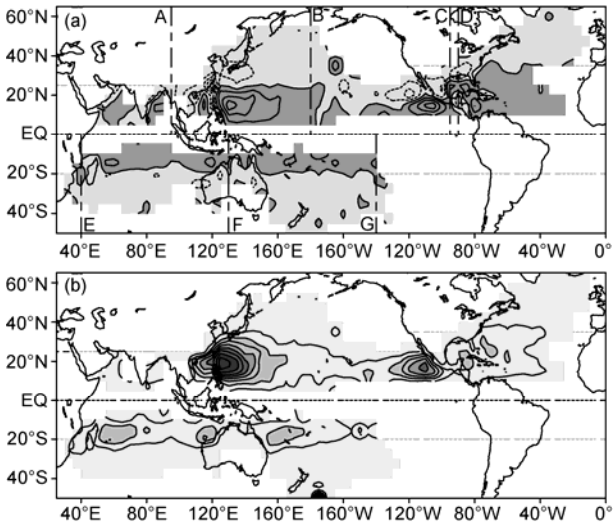

Figure 1 The climatological distribution of the TC activity indices during 1951–2008. (a) The accumulated energy increment (AEI), with positive regions in orange and negative regions in light blue. Contours are at intervals of 5×10^2 m^2, and the thick solid line indicates AEI = 0 m^2. The vertical blue short-long-dashed lines labeled by A–G indicate different ocean basins, that is, the western North Pacific (WNP) basin between A and B (95°E–180°), the eastern North Pacific (ENP) basin between B and D (180°–90°W), the North Atlantic (ATL) basin to the east of C (0°–95°W), the South Indian Ocean (SIO) basin between E and F (40°–130°E), and the western South Pacific (WSP) basin between F and G (130°E–180°–140°W). (b) the accumulated cyclone energy (ACE), with contour interval of 3×10^3 m^2. Dot gray lines in both plots are for latitudes of 20°S, 25°N, 35°N, and the Equator.

the energy sinks are quite broad in the extratropical areas over other four basins, that is, the western North Pacific (WNP), the North Atlantic (ATL), the South Indian Ocean (SIO), and the western South Pacific (WSP). The borderlines between the sources and sinks, where AEI is equal to zero, are close to the 20°S in either SIO or WSP, close to 25°N in WNP, and close to 35°N in ATL. Although the actual latitudes of the borderline are different among the four basins, they are all in subtropics. Therefore, the translations of TCs across the borderline transport energy from the tropics to the extratropics.

2.2 Seasonality

The annual cycle of AEI exhibits unique characteristics of the seasonality of TC activity over different ocean basins.

First, as indicated by the monthly evolution of AEI distribution (Figure 2), the energy sources and sinks in the WNP exist in all months, with the smallest area and amplitudes limited to the east of the Philippines in February (Figure 2(b)) and the largest area and amplitudes in August to November (Figure 2(h)–(k)). Over the open ocean region, the borderline between the energy source and sink shifts northward and southward seasonally and reaches the highest latitude, about 30°N, in August. The seasonal expansion of the energy source of TC activity seems very similar to the seasonal meridional migration of East Asian monsoon, which implies there may be a close relationship between them.

The seasonality of TC activity is quite different in ATL although there is also extratropical energy sink in the basin. The energy sources are only obvious during June to November (Figure 2(f)–(k)), covering the largest area in August and September. With differences from the WNP basin, the energy source appears firstly along the Gulf Stream (Figure 2(f)), then two sources appear both over the Caribbean Sea and the Gulf Stream (Figure 2(g)), after that, the two sources merge together (Figure 2(i)), and then the sources are broken up and weakened (Figure 2(j)–(k)).

In the other two basins of the north hemisphere, the ENP and BIO, both the energy sources and sinks are limited to the tropics, and the features of seasonality are also unique for either of them. In the ENP basin, the source and sink are obvious during May to November with the peaks in August (Figure 2). The seasonal westward expansions and contractions of both the source and sink are more obvious than their meridional expansions. In August, both the source and sink in ENP merge with the source and sink in the WNP, respectively, and then withdraw eastward. On the other hand, the annual cycle of TC activity over the BIO has two peaks in May and November [22]; the associated energy source and sink are also obvious during the two months although their areas are smaller than any other basins.

The active TC season for both basins in the south hemisphere is from October to next May, and both the energy sources and sinks are obvious during December to next April (Figure 2(a)–(e) and (j)–(l)). Although the two austral basins are broad, the energy sources of TC activity are all limited to the regions within 20°S, while the sinks expand poleward seasonally, and extend most south to the midlatitudes (Figure 2(b) and (c)).

The seasonal variations of TC energy sources and sinks further suggest that the zonal asymmetry of TC activity is more significant in the north hemisphere than that in the south hemisphere. Therefore, it is easy to hypothesize that the features of TC activity may be associated with the distribution of global continents and oceans.

3 The influences of land-sea thermal contrast on TC energy sources and sinks

Figure 1 suggests that the asymmetries of the TC activity regions are not only between the north and south hemispheres, but also between different longitudes. In contrast, according to some numerical simulations by the aquaplanet general circulation models with moist process, when SSTs were in zonally symmetric distribution, there were no obvious zonal asymmetries in distributions of both the convective available potential energy and the precipitation [51, 52], and TC-like storms could generate in any place of the tropics [51]; meanwhile, when SSTs are in zonally asymmetric distribution, the distributions of both the wind of 850 hPa and precipitation were zonally asymmetrical, and the maximum precipitation rate was usually on the side of low level westerlies close to the convergence zone of easterlies and westerlies [53]. These results confirm that the geographic distribution of TC activity is closely related to the land-sea thermal contrast.

3.1 The dominant diabatic heating in the energy sources and sinks of TC activity

The condensation heating of deep convection is significant mainly in low latitudes, and the TC activity also contributes to it. As reported in literatures, TC-induced precipitation accounts for about 4% of the annual total precipitation over ATL and ENP, and about 12% over the WNP [54–56]. This suggested that most of the condensation heating was not induced by TC activity, and this is the environment of TC activity.

The condensation heating of deep convection is also asymmetric between the north and south hemispheres and between different longitudes (Figure 3). In the austral summertime (December to next April, DJFMA), the column-integrated apparent heat source $<Q_1>$ and apparent moisture sink $<Q_2>$ have similar patterns: both are positive in the energy sources of TC activity and negative in the sinks (Figure 3(a) and (b)), which indicates that the CO is dominant heating in the sources while LO is dominant in the

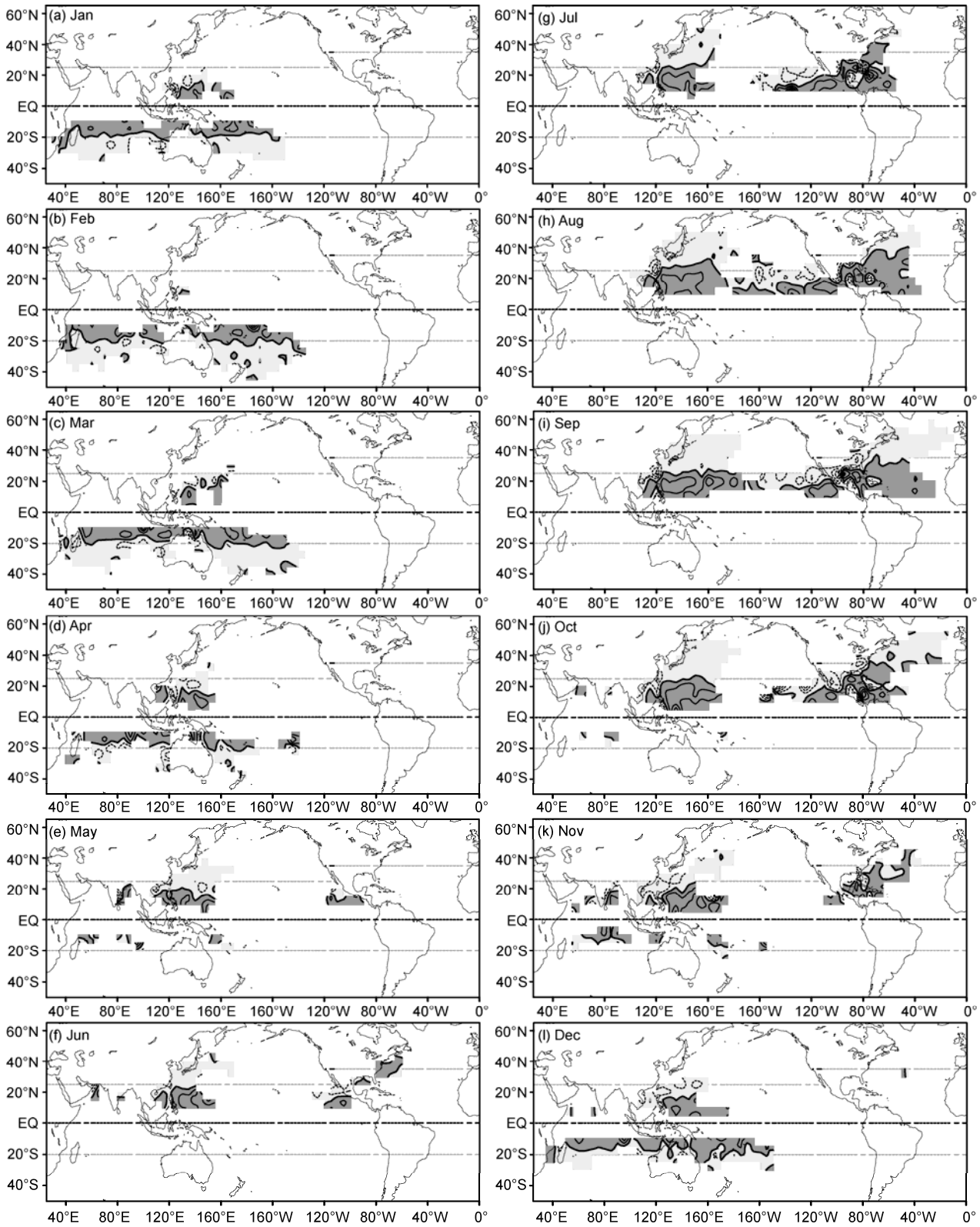

Figure 2 Same as in Figure 1(a), but for climatological monthly AEI during 1951–2008. Contours are at intervals of 5×10^2 m^2.

sinks. In the boreal summertime (May to October, MJJASO), the distributions of $<Q_1>$ and $<Q_2>$ are similar in Asian monsoon region and the area from the warm region of ENP to the Gulf of Mexico but different over the open ocean of ATL (Figure 3(c) and (d)), which indicates that CO dominates in the former regions but SE dominates in the latter region. The results are further confirmed by the vertical cross sections of Q_1 and Q_2 in the summertime tropics (Figure 4). Over the open ocean of ATL, Q_1 is positive in the near surface level and negative above it, which indicates cooling of the air column above the surface SE (Figure 3(c)). Meanwhile, Q_2 is negative below 700 hPa, suggesting the low levels sinks of moisture. The moisture sinks are actually the low stratiform clouds in the sub-inversion layer due to the condensation of water vapors evaporated from the ocean. Similar characteristics can also be found between 120°W and 160°W since the energy sink of ENP TC activity is dominant in latitudes of 5°–25°N.

Figure 5 shows the vertical heating profiles in either the energy sources or the sinks of TC activity. The energy sources and sinks are distinguished by the borderlines of zero AEI in the Figure 1(a), and the ocean basins are also defined as in Figure 1(a). As shown in Figure 5, the total heating is very small in the energy sinks, and the magnitude of LO is about double of the CO with exception in ENP basin, which indicates the dominant role of LO in energy sinks of TC activity. In contrast, the CO is much intense in the energy sources and the total heating is positive in upper troposphere. Such characteristics are especially typical in the WNP basin and the two south hemispheric basins, with total heating about 2 K d^{-1} in comparison with total heating less than 1 K d^{-1} in either ENP or ATL basins where the CO

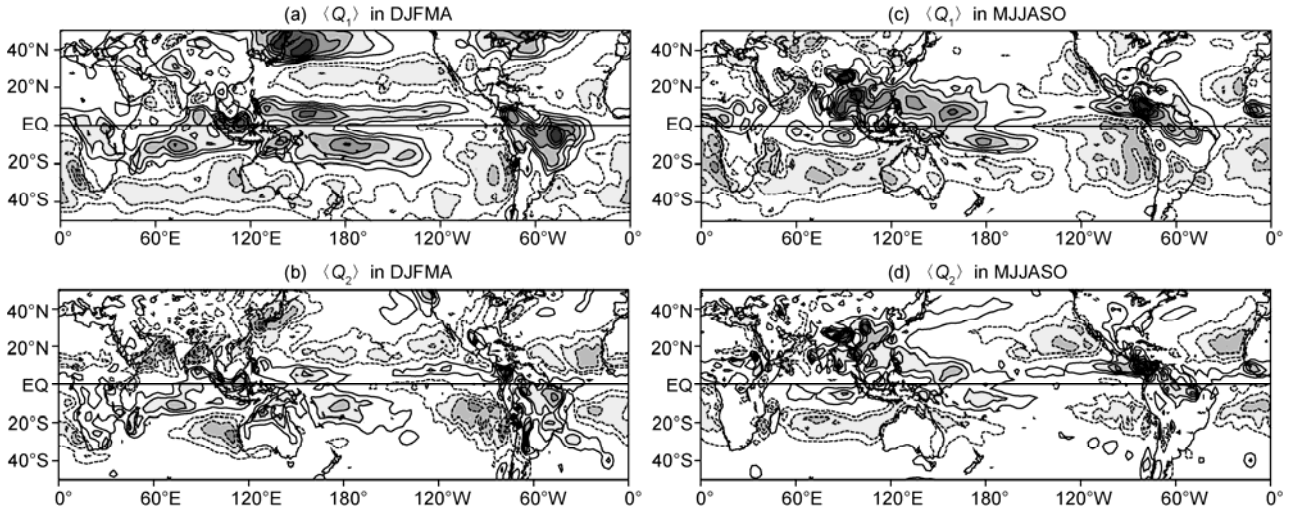

Figure 3 The column-integrated apparent heat source $<Q_1>$ and apparent moisture sink $<Q_2>$ during December to next April (DJFMA) and May to October (MJJASO). Contours are at intervals of 50 W m^{-2} and the line for zero is omitted.

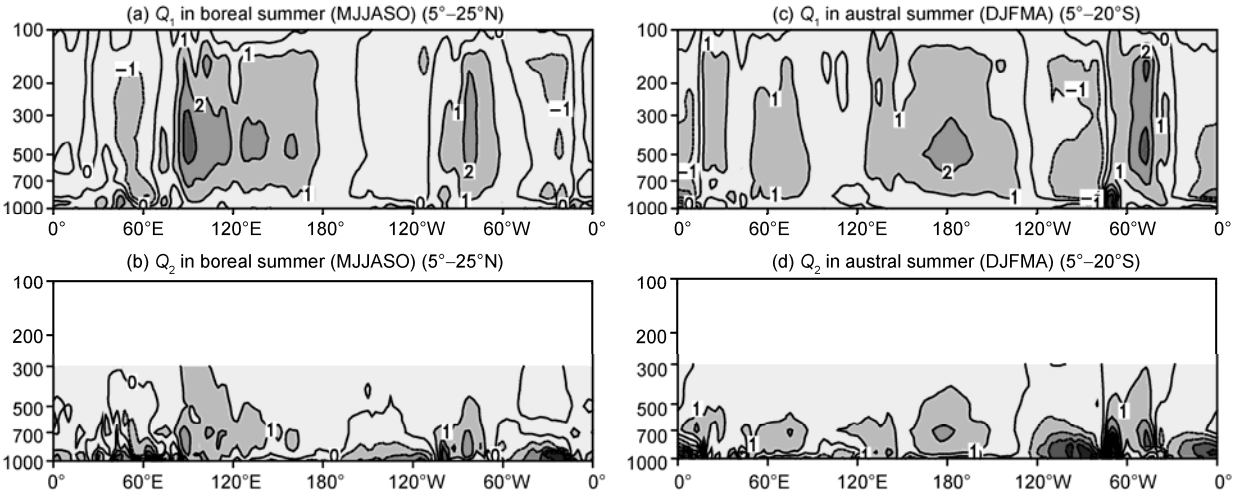

Figure 4 The vertical cross sections of apparent heat source Q_1 and apparent moisture sink Q_2 over the boreal tropics (5°–25°N) during the boreal (MJJASO) and austral summertime (DJFMA). Contours are at intervals of 1 K d^{-1}.

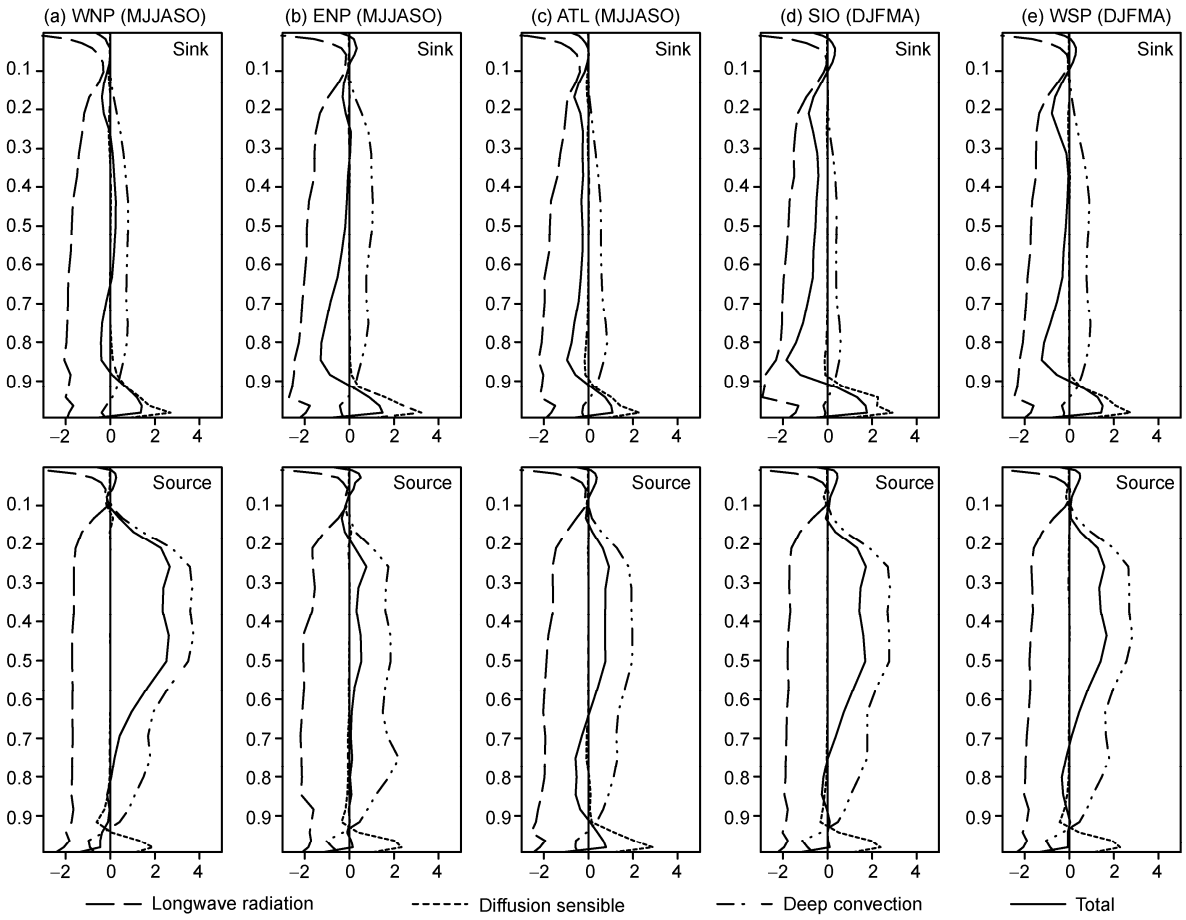

Figure 5 The vertical profile of different diabatic heating (K d^{-1}) for the energy sources and sinks of TC activity during MJJASO and DJFMA for boreal and austral summer, respectively. The vertical coordinate is σ-coordinate. (a) WNP (95°E–180°), (b) ENP (90°W–180°), (c) ATL (0°–95°W), (d) SIO (40°–130°E), (e) WSP (130°E–180°–140°W).

is almost equal to LO. It should be noted that the characteristics of energy source and sink in ENP, separated here by the borderline of zero AEI in Figure 1(a) may be mixed up because of their zonal expansion and contraction and the sink within the tropics (Figure 2). With the knowledge of Figure 3(c) and (d), the CO is the actual dominant heating in the energy source in ENP basin.

Overall, the energy source of TC activity is characterized by the double dominant heating of LO and CO in the ATL basin but characterized by CO in the rest basins. Moreover, the column-integrated total heating is positive in the sources but negative in the sinks (as shown in Figure 3(a) and (c)), which indicates net heating in sources and net cooling in sinks. Therefore, the translations of TCs, from the energy sources where TCs extract energy from the environment to the sinks where TCs return energy to the environment, are one of the mechanisms of energy redistribution. Moreover, the definition of AEI based on the best track data is also validated as the energy source and sink are consistent with the distribution of diabatic heating.

3.2 The impacts of the quadruplet heating pattern in subtropics

The summertime subtropics are characterized by the LOSECOD quadruplet heating pattern associated with the land-sea thermal contrast: the LO dominates over the eastern part of ocean while double dominant heating is typical over the western part of ocean [4–6]. Moreover, the distribution of CO in the tropics is also asymmetrical: the CO expands to the subtropics over the western part of ocean while the subtropical LO expands largely to the tropics and the CO is limited to narrow band close to the Equator over the eastern part of ocean (Figures 3 and 4). The energy sources of TC activity are consistent with the region of CO, which indicates the potential influences of land-sea thermal contrast on the asymmetrical distribution of TC energy sources.

For different pattern and different kind of diabatic heating, the associated atmospheric circulation will be different [57, 58]. In general, there may be upper level anticyclonic vorticity above the low level cyclonic vorticity on the western side of CO, and vice versa on the eastern side; mean-

while, the LO may induce upper level cyclonic circulation over the low level anticyclonic circulation. As inferred from Figures 3 and 4, the CO is more intense over the western part of the ocean while LO is more intense over the eastern part. Consequentially, there are upper level anticyclonic vorticity and the low level cyclonic vorticity over western part of ocean, and vice versa over the eastern part of ocean (as shown in left panel of Figure 6). The vertical pattern of vorticity over the western part of ocean is more favorable for TC activity and poleward motion than that over the eastern part. Therefore, over the western part of the ocean, TC activity is more active and its energy sink is broader (Figure 1). Obviously, the LOSECOD quadruplet heating pattern, especially the parts over the ocean, modulates the energy sources and sinks of TC activity into zonally asymmetrical ones.

Moreover, because of the discrepancies in width of the oceans, the details of LOSECOD pattern over the North Pacific are different from those over the ATL. In particular, the intense LO and CO are distinguished clearly with the former over the ENP and the latter over the WNP, while they lap over with each other over the ATL. Therefore, the LO dominant region elongates zonally to the north of the CO dominant zone over the WNP, while over the ATL, the LO dominant region is to the northeast of the CO dominant region with borderline across the latitudes (as shown in Figure 4(c) and (d)). The different patterns of diabatic heating result in different environments for TC activity and its seasonality, which will be discussed further in section 4.

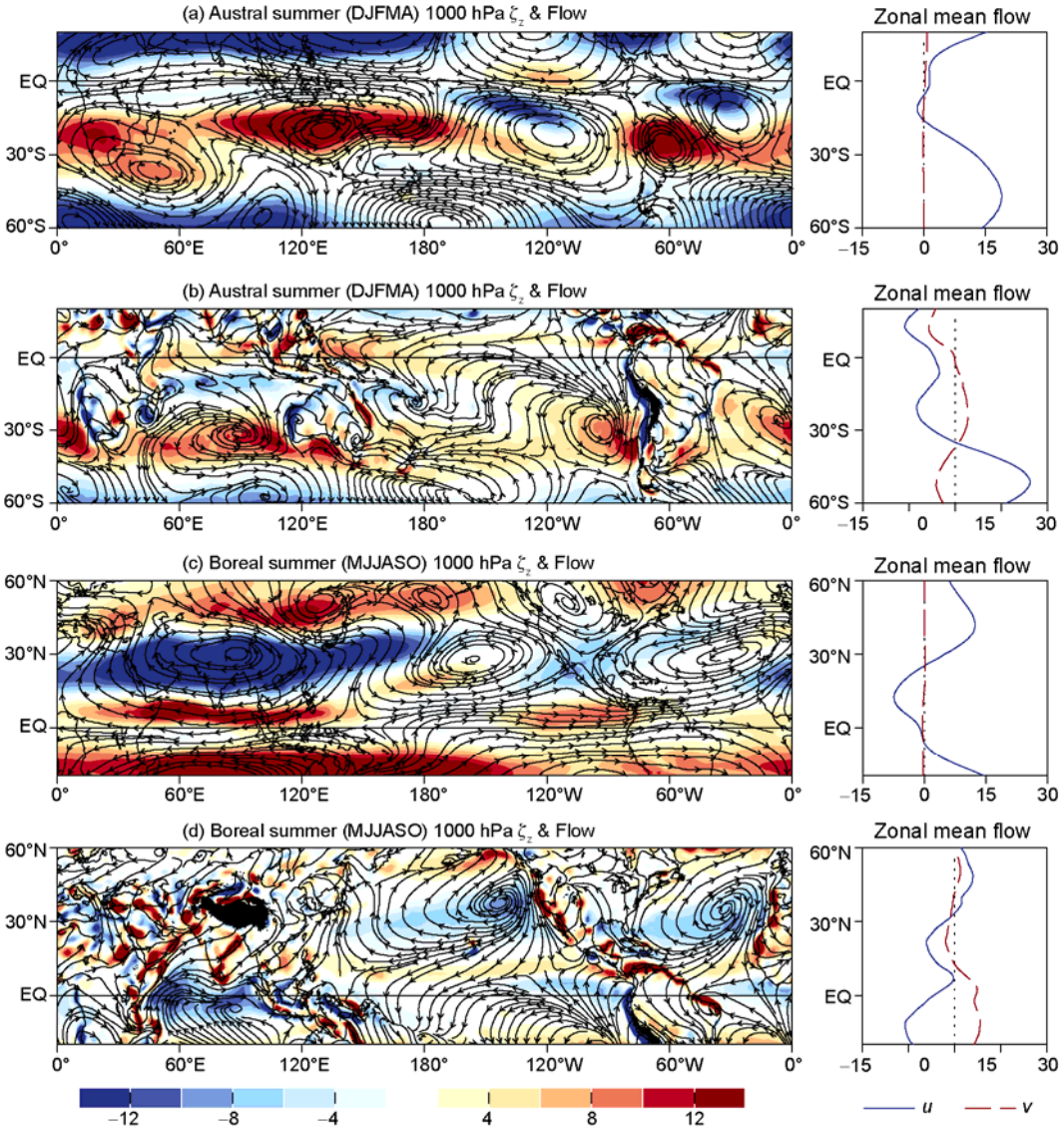

Figure 6 The summertime relative vorticity (10^{-6} s^{-1}, shaded) and deviation of streamline from the zonal mean at 100 and 1000 hPa, respectively (left panel); and the corresponding zonal mean wind velocity (m s^{-1}, right panel). Terrain with elevation higher than 3 km is shaded with black color.

3.3 The impacts of the tropical asymmetric diabatic heating pattern

Although the oceans account for the most part of the tropics, the heat contents are alternated because of the barriers of land and islands, and seawater is warmer in the western part of the ocean than the eastern part [23, 24]; consequentially, both the air-sea interaction and diabatic heating in the tropics are zonally asymmetrical (e.g. Figures 3 and 4).

The right panel of Figure 6 indicates that the summertime zonal mean flow is different between the north and south hemispheres. In austral summer, the mean flow is mainly easterlies in low level of the tropics while it is weak at 100 hPa. In contrast, the mean flow is dominant by the easterlies in both the upper and low levels of the tropics in boreal summer. Moreover, even in the same season, the tropical circulations of upper and low levels are different with some easterly and some westerly vertical shear regions (as shown in left panel of Figure 6). The vertical shear, which is an important factor affecting the TC genesis and development [11, 14], here is defined by the wind vector of 200 and 850 hPa:

$$\vec{V}_{\text{shear}} = \left(U_{\text{shear}}, V_{\text{shear}}\right) = \left(\frac{U_h\big|_{P_u} - U_h\big|_{P_b}}{\left|P_u - P_b\right|}, \frac{V_h\big|_{P_u} - V_h\big|_{P_b}}{\left|P_u - P_b\right|} \right), \quad (4)$$

where $\vec{V}_{\text{shear}}$ is the shear vector, U_{shear} and V_{shear} are the zonal and meridional components of shear vector, respectively, U_h and V_h are the zonal and meridional wind components, respectively. P_u = 200 hPa, P_b = 850 hPa.

As shown in Figure 7, there are broken regions of easterly vertical shear (EVS) in both hemispheres. In austral summertime, the EVS is over the western part of the South America and the tropics of eastern hemisphere, and the core is close to 5°S. Meanwhile, the more intense EVS is over the warm ocean surface of ENP and the region from the eastern Atlantic to 160°E, with the core located on 5°–10°N. With the knowledge of diabatic heating in Figure 3(a) and (c), the regions of summertime EVS in both hemispheres overlap with the tropical diabatic heating with westerly shear at the western and eastern sides. This results from the Gill-type response of the tropical circulation to the asymmetric diabatic heating about the Equator [59].

The EVS is important for TC activity. On the northeastern edge of the EVS region, the vertical shear vectors change anticyclonically (Figure 7), which are favorable for TC activity as anticyclonic circulation in upper level and cyclonic circulation in low level; while on the adjacent edge of the westerly vertical shear region, the shear vectors change cyclonically indicating anticyclonic circulation in upper level and cyclonic circulation in low level, which are unfavorable for TC activity. In other words, even the vertical shear is weaken, the influence of its change, anticyclonic or cyclonic, on TC activity is not equal. Moreover, over the austral summertime EVS region from the tropical SIO to WSP, the shear vectors change anticyclonically (Figure 7(a)). The related region favorable for TC activity is consistent with the energy sources defined by the AEI (Figure 1(a)). It is similar for the summertime North Pacific Ocean (Figure 7(b)), the energy sources of both ENP and WNP are associated with the anticyclonical change of shear vectors. On the other side, the large shear is also consistent with the double dominant heating of the energy source (Figures 3(c) and (d), 4 and 5(c)). Overall, the northeastern edge of the EVS region, which is induced by the zonally asymmetric diabatic heating associated with distribution of continents and oceans, is favorable for TC activity. Moreover, it is consistent with both the monsoon region [60] and the warm SST (>28°C, Figures are not shown) region which are favorable for deep convections. This suggests that the TC activity may be modulated by the ocean-land-atmosphere interactions.

Aside from the EVS region, the low level westerlies are also significant over the Africa and the equatorial region from the Indian Ocean to the western Pacific (Figure 8), and the most intense westerlies is over the latter region and extends to 500 hPa. Webster and Chang [61] indicated that the equatorial energy accumulation and emanation region were located east to the maximum westerlies. Statistics on TC genesis locations suggested that the initial perturbulance of TCs are consistent with the energy accumulation regions, not only for the WNP and Indian Ocean but also for the north Africa where the original perturbulance of ATL TCs (the North Africa easterly waves) come from [22, 62]. Meanwhile, as shown in Figure 1(a), on the northeastern side of the low level westerlies of the Indian–western Pacific Ocean, both the energy source and sink of the WNP are the most intense worldwide, which suggests the most active translation of TCs from the energy source to the sink. This is also consistent with the emanation region suggested by Webster and Chang [61].

The CO suggests large freshwater flux from the ocean and plenty of deep convections, and vice versa for LO. However, even in CO dominating region, only a part of the CO is attributed to the TC activity [54–56]; in other words, only a part of the deep convections is organized into TCs, This may due to the limitation of atmospheric dynamical conditions, such as low level vorticity, wind shear, favorable region for energy accumulation and so on. According to the results discussed previously, these dynamical conditions are closely related to the atmospheric responses to both the diabatic heating pattern over the subtropics and tropics. Therefore, variations of the dynamical conditions may be one of the approaches through which the land-sea thermal contrast modulates the geographic distribution of TC activity.

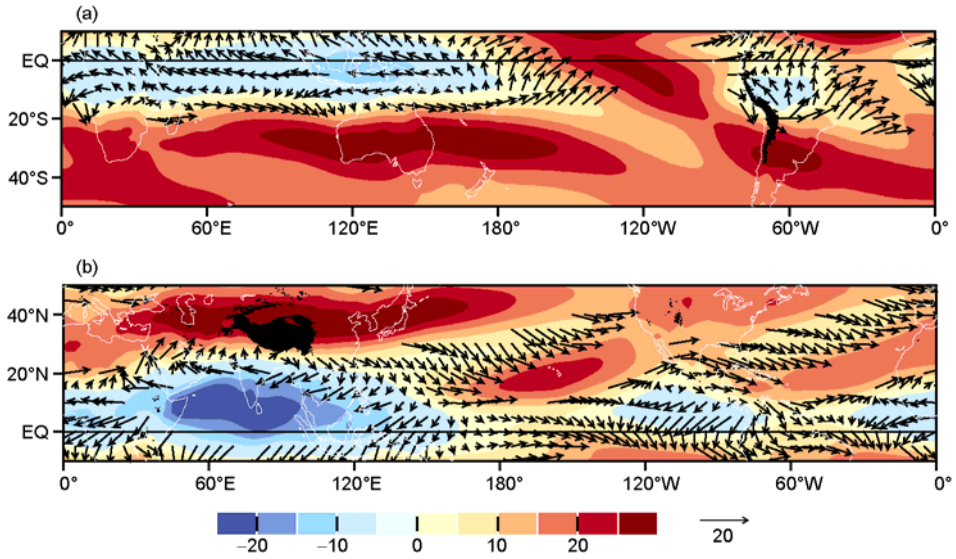

Figure 7 The vertical shear vector ($\bar{V}_{shear}$ < 12 m s^{-1}/650 hPa, vectors) of 200–850 hPa and its zonal component (U_{shear}, in m s^{-1}/650 hPa, shaded). (a) The austral summer DJFMA; (b) the boreal summer MJJASO. Terrain with elevation higher than 3 km is shaded with black color.

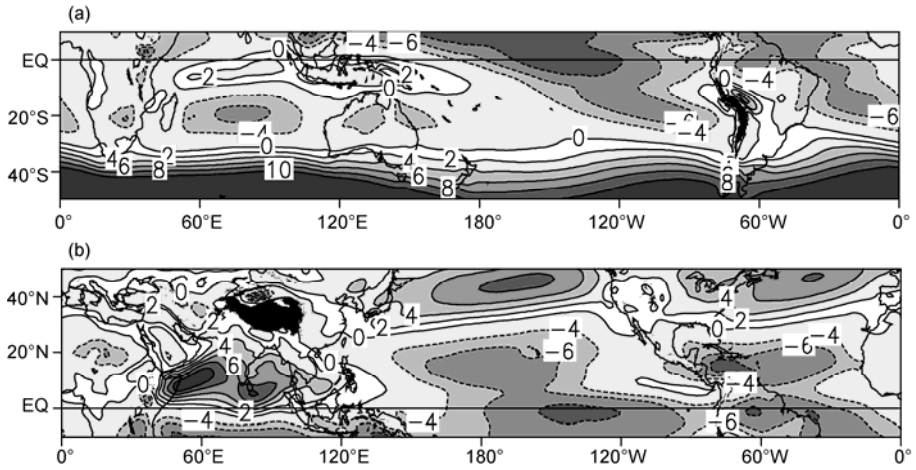

Figure 8 The zonal wind of 850 hPa (m s^{-1}). (a) The austral summer DJFMA; (b) the boreal summer MJJASO. Terrain with elevation higher than 3 km is shaded with black color.

4 The impacts of the diabatic heating pattern on the seasonality of TC activity

With reference to the results in section 3.1, the distributions of energy source and sink over the oceans with different width are different in details. For instance, they are different over the WNP and ATL. On the other hand, results in section 2.2 suggest the seasonality of TC activity is also different from basin to basin. In this section, we will focus on the unique seasonality of TC activity over different ocean basins.

First, the monthly evolution of CO and LO for three ocean basins, the WNP, ENP and ATL, are shown in Figure 9. As pointed out in section 3.2, the North Pacific is in large width, and the centers of LO and CO are over the eastern and western part of the ocean, respectively. As far as the seasonality of TC activity is considered, the monthly evolution of the diabatic heating of the energy source is quite consistent in longitudes of the WNP (Figure 9(a)); however, the variation of CO is in contrast to the LO, with weaker CO and more intense LO until May, and vice versa since July. That is the reason why the seasonal expansion of energy source over WNP is in-phase basin-wide (Figure 2). The two basins in the South Hemisphere are similar to the WNP although it is not so significant as WNP since the land-sea contrast is not so significant as the North Hemisphere.

As pointed out in section 3.1, the energy source of TC activity over the ATL is dominated by both CO and LO. Moreover, Figure 9(b) suggests that there are sub-basin scale characteristics. Over the narrow band to the west of

60°W, the monthly evolutions of CO and LO are consistent with the WNP, while to the east of 60°W, LO is more intense than CO, and the LO dominated region expands westward seasonally. Accordingly, the low level anticyclonic and upper level cyclonic circulation, which is unfavorable for TC activity, is induced in response to the intense LO. The unfavorable region expands westward as LO enhanced in summertime, causing the region favorable for development of initial eastern waves smaller. Therefore, TC genesis in ATL is not as easy as in WNP. The seasonal variation of energy source in ATL is due to the unfavorable atmospheric conditions associated with the evolution of diabatic heating. Moreover, some of the easterly waves are prevented from well developing over the ATL. These easterly waves enter the ENP and develop over the warm ocean surface, inducing a more intense TC activity than the ATL (Figure 1(b)).

The seasonal variation of the energy source over the ENP is also influenced by LO. As shown in Figure 9(c), the CO dominant region contracts westward since May while the LO dominant region expands synchronically; and both reach the most western longitude in October. The seasonal variations of the CO and LO are consistent with the energy source of TC activity for the ENP basin (Figure 2).

The seasonality of BIO is different from any of the other ocean basins by its unique bimodal feature. The strong vertical shear associated with summer monsoon is unfavorable for TC activity. Compared with the active monsoon season from July to August, the distributions of diabatic heating in active TC seasons, May and November, are different from the monsoon season by the heating over the subcontinent of South Asia (Figure 10). Specifically, for the active TC season, the subcontinent is dominated by SE with LO and D zones over the Arabian Sea and CO and D zones over the Bay of Bengal (Figure 10(a) and (c)), whereas the subcontinent is dominated by CO in the active summer monsoon season (Figure 10(b)). Moreover, the heating patterns are different even in the two active TC months of May and November since the seasonal background is different.

For the first active TC season of May, the atmospheric circulation is transitioned from winter pattern into summer pattern. During this month, the strong Somalia cross equatorial jet is over the Somalia, and the Asian monsoon is onset firstly in the Bay of Bengal [63] accompanied with strong CO. The CO enhances the low level westerlies on its western side, and the near-equatorial BIO is dominated by the westerlies. On the other side, the strong SE over the Araby and Somalia induces the cyclonic vorticity in the low troposphere, which in turn results in one branch of the cross equatorial flow turn to southeasterly over the Red Sea and South Araby. Meanwhile, SE is very strong over the subcontinent of South Asia while LO dominates the Arabian Sea and CO dominates the Bay of Bengal, which is similar to the summertime LOSECOD quadruplet heating pattern in the subtropics (Figure 10(a)). According to Wu and Liu [57] and Liu et al. [58], such pattern of diabatic heating may result in cyclonic circulation in low levels and anticyclonic circulation in upper levels (Figure 10(a)), which in turn induces cyclonic vorticity and makes the another branch of the cross equatorial flow turn to southwesterly when it cross the south part of the subcontinent. During this month, the vertical shear is small over the BIO and there are anticyclonic shear vectors over the Arabian Sea and the marginal sea east to the subcontinent (Figure 10(a)), and both are favorable for TC activity.

During the active monsoon season of July and August, the diabatic heating over the subcontinent and surrounding ocean is dominated by CO, with the intensity stronger than 180 W m^{-2} and the area about 25°×25° (Figure 10(b)). As shown in Figure 4(a), the heating is stronger than 3 K d^{-1} in

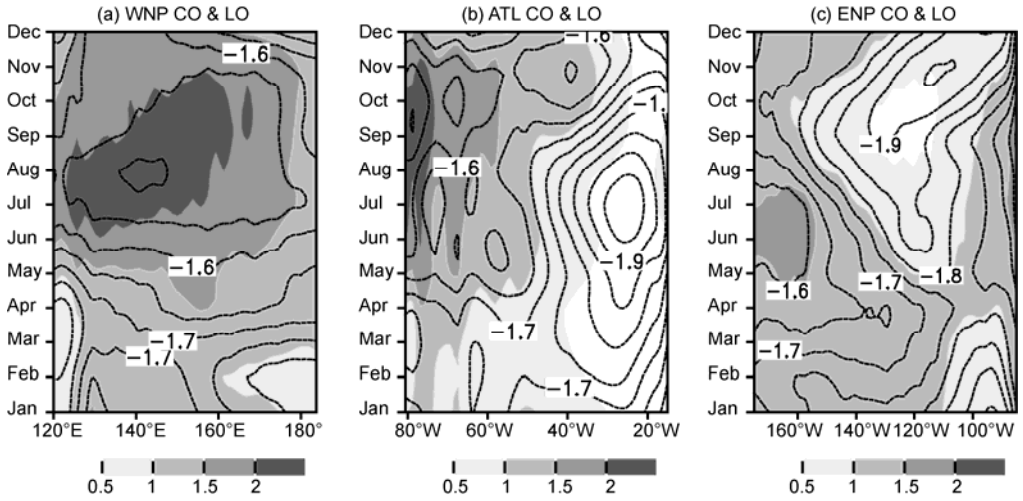

Figure 9 The monthly evolution of column-integrated condensation heating (W m^{-2}, shaded) and radiative cooling (W m^{-2}, contour). (a) WNP (EQ–25°N); (b) ATL (EQ–35°N); (c) ENP (EQ–10°N).

the mid-troposphere of 500–300 hPa. It results in strong low level cross equatorial flow and westerlies on the western side of heating center, and a cyclonic circulation on the northwestern side (Figure 10(b)), which is the typical Gill-type response to the asymmetric heating [59]. Meanwhile, the CO results in strong easterlies and equatorward flow, and anticyclonic circulation on the northwestern side of its center in the upper troposphere. Moreover, over the western Africa and Araby, SE is very strong, enhancing the low level westerlies and upper level easterlies. With the effects of both the SE and CO, the vertical shear is strong and the shear vectors change cyclonically both over the Arabian Sea and almost all the Bay of Bengal (Figure 10(b)), which are unfavorable for TC activity. Therefore, the results indicate that the different circulation patterns, which are induced by the different diabatic heating patterns over the BIO and surrounding continents, influence the atmospheric conditions favorable for TC activity and in turn cause different TC activity in different seasons over the BIO.

For the second active TC season of November, the atmospheric circulation is transitioned from summer pattern into winter pattern, with westerlies to the south of the Tibet Plateau, easterlies over the middle of BIO, and cross equatorial into the south hemisphere (Figure 10(c)). Meanwhile, not only the SE of the subcontinent, the Araby and Somalia is weaker than May, but also the LO over the northern part of the Arabian Sea is weaker, too. The associated circulation is more obvious in the low levels with anticyclonic vorticity over the region from the subcontinent to the Araby. On the other hand, the strong CO is only on the southern part of the Bay of Bengal, with D zone to the north of 15°N. The CO induces low level westerlies and upper level easterlies close to the Equator, and low level cyclonic circulation and upper level anticyclonic circulation over the southern part of BIO. The vertical shear is weaker than the active monsoon season while the shear vectors changes anticyclonically, and both are favorable for TC activity. Overall, differing from the active monsoon season, the subcontinent is dominated by the SE during both active TC seasons although the intensity of SE is different between the two active TC seasons. With respect to the modulation of diabatic heating pattern on the regional circulation, the combined LO-SE and CO pattern is important for the favorable conditions of TC activity in May, while the CO close to the Equator is the essential factor for the favorable conditions in November.

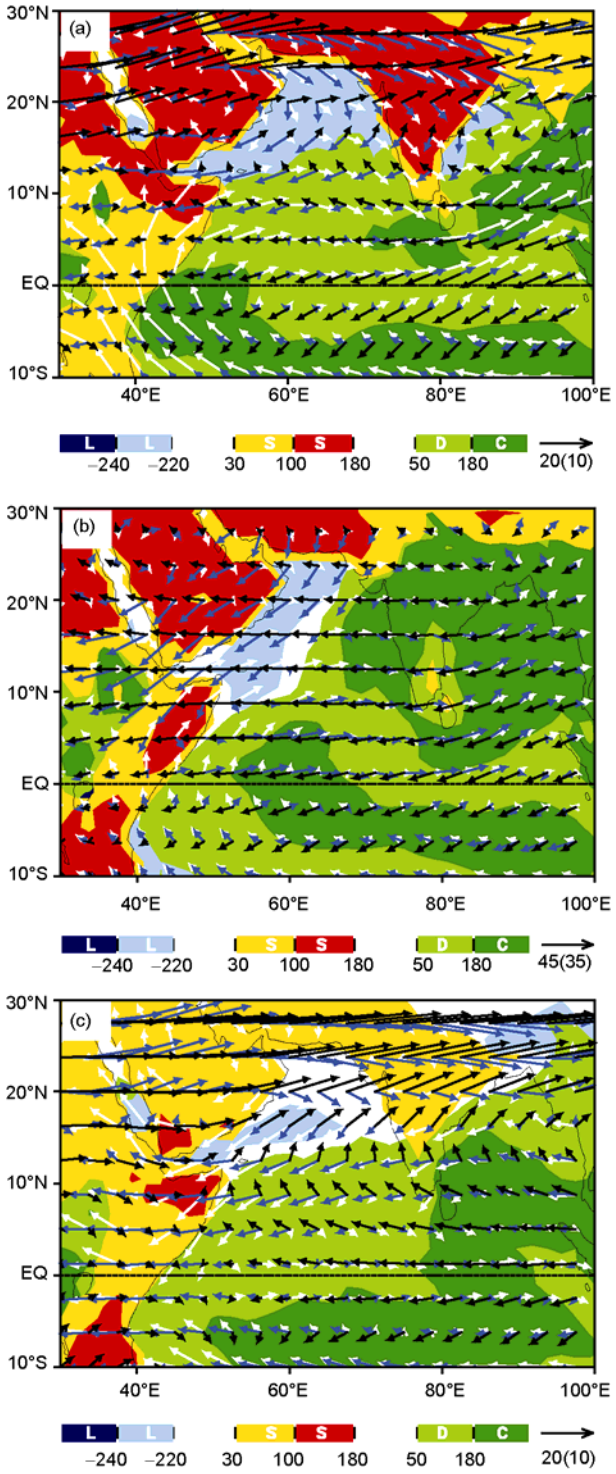

Figure 10 The main local column-integrated diabatic heating (W m^{-2}, shaded) and wind (m s^{-1}, vector) of 200 (black), 500 (blue) and 850 hPa (white) over the BIO region. (a) the first active TC season (May), (b) the active monsoon season (July to August), and (c) the second active TC season (November). The scale of vector without the parentheses is for wind of 200 hPa, while scale of vector within the parentheses is for both 500 and 850 hPa. On the color bar, L denotes radiative cooling, S denotes sensible heating, C denotes condensation heating, and D denotes double dominant heating.

5 Concluding remarks

In this paper, the accumulated energy increment (AEI) index is defined using the TC best track data. The AEI index demonstrates the unique characteristics of energy sources and sinks of TC activity over different ocean basins, both the geographic distribution and its seasonality, which are

related to the influences of diabatic heating pattern associated with the distribution of continents and oceans.

The energy sources identified by the distribution of AEI are characterized by diabatic heating of CO and D, the double dominant heating of CO and LO, while the sinks are characterized by LO. This subtropical LOSECOD quadruplet heating pattern, associated with the land-sea thermal contrast, results in favorable vorticity pattern over the western part rather than the eastern part of the ocean, and in turn results in the differences of TC activity between the two parts of ocean. With different zonal width of the ocean, the mutual influences between the diabatic heating over the western and eastern part of the ocean are different, which induces the different characteristics of TC activity either over the WNP or the ATL. Moreover, the tropical asymmetric diabatic heating pattern also results in the most intense easterly vertical shear and low level westerlies over the region from equatorial Indian Ocean to the WNP. The former induces favorable vertical shear in the energy source of TC activity while the latter is favorable for the energy accumulation and emanation in the WNP basin, and both are favorable for the most intense energy source and sink of TC activity of WNP among global ocean basins.

The seasonality of TC activity is also modulated by the land-sea thermal contrast through its influences on the energy sources and sinks. In particular, the TC activities over the WNP, SIO and WSP are similar to the meridionally seasonal expansion and contraction of the energy sources and sinks associated with the variation of diabatic heating. On the other hand, both TC activities over the ATL and ENP are influenced by the strong LO, except that the former is characterized by seasonal merger and breakup of the energy source, while the latter is characterized by zonally seasonal expansion and contraction of the energy source and sink. The annual cycle of TC activity over BIO, with two different peaks, is also closely related to the variation of diabatic heating.

In summary, the land-sea thermal contrast is the essential factor inducing the discrepancies of TC activity in different ocean basins, such as the geographic distribution, intensity of activity, seasonality, and so on. Although only the climatology of land-sea thermal contrast is discussed in this paper, it can be inferred that its variation may also have influences on TC activity. Moreover, once the variation of land surface thermal condition is considered, the influences of biosphere and anthropogenic activity would be taken into account. By this point, TC activity, as one of the mechanism of energy redistribution, may have more comprehensive relationship with different components of the climate system.

Appendix A: Influences of TC size on definition of AEI

Currently, the global TC size data are incomprehensive; therefore, neither temporal nor spatial variations of the TC energy can be estimated accurately. In this appendix, we attempt to analyze the influences of TC size on the definition of AEI. According to Mallen et al. [50], and the radius r and tangential wind speed V are written as

$$r = R_{\mathrm{MW}}\tilde{r},\quad V = V_{\max}\tilde{V},$$

where $V_{\max}$ and R_{MW} are the MSW and corresponding radius, respectively, and $\tilde{V}$ and $\tilde{r}$ are dimensionless wind speed and radius, respectively. The $V_{\max}$ and R_{MW} are actually the typical wind speed and radius of TC, respectively. Using the Rankine vortex as approximation of TC

$$V(r) = \begin{cases} r & r \leqslant 1, \\ r^{-\alpha} & r > 1, \end{cases}$$

where $0 \leqslant \alpha \leqslant 1$ are the decay parameter, which can be estimated from the radial wind profile data observed by aircraft reconnaissance.

For a particular time, the net production of mechanical energy of TC, P, and the net energy dissipation, D, are [64]

$$\begin{aligned} P &= 2\pi \frac{T_{\mathrm{s}} - T_{\mathrm{o}}}{T_{\mathrm{s}}} \int_0^r \left[C_k \rho |V| \left(k_0^* - k\right) + C_D \rho |V|^3 \right] r \mathrm{d}r \\ &= 2\pi \frac{T_{\mathrm{s}} - T_{\mathrm{o}}}{T_{\mathrm{s}}} V_{\max} R_{\mathrm{MW}}^2 \int_0^1 C_k \rho \left(k_0^* - k\right) \left|\tilde{V}\right| \tilde{r} \mathrm{d}\tilde{r} \\ &\quad + 2\pi \frac{T_s - T_o}{T_s} V_{\max}^3 R_{\mathrm{MW}}^2 \int_0^1 C_D \rho \left|\tilde{V}\right|^3 \tilde{r} \mathrm{d}\tilde{r} \end{aligned}$$

and

$$\begin{aligned} D &= 2\pi \int_0^r C_D \rho |V|^3 r dr \\ &= 2\pi V_{\max}^3 R_{\mathrm{MW}}^2 \int_0^1 C_D \rho \left|\tilde{V}\right|^3 \tilde{r} \mathrm{d}\tilde{r}, \end{aligned}$$

respectively. This indicates that both P and D are functions of R_{MW}, $V_{\max}$, and the profile of $\tilde{V}$. In the formulae of P and D, T_{s} is the sea surface temperature, T_0 the temperature of TC's outflow, C_{k} and C_{D} the air-sea exchange coefficients. According to Mallen et al. [50], the profile of $\tilde{V}$ for different TC has a similar shape (as shown in their Figure 4(a)) and thus can be seen as steady in both time and space. Therefore, the essential parameters that determine either P and D are R_{MW} and $V_{\max}$; that is,

$$P = ab_1 V_{\max} R_{\mathrm{MW}}^2 + ab_2 V_{\max}^3 R_{\mathrm{MW}}^2,$$

$$D = b_2 V_{\max}^3 R_{\mathrm{MW}}^2,$$

where $a = \left(T_s - T_o\right)/T_s$, $b_1 = 2\pi \int_0^1 C_k \rho \left(k_0^* - k\right) \left|\tilde{V}\right| \tilde{r} \mathrm{d}\tilde{r}$, and $b_2 = 2\pi \int_0^1 C_D \rho \left|\tilde{V}\right|^3 \tilde{r} \mathrm{d}\tilde{r}$. Define $E=P-D$ as the net energy increment, we have

$$E = \left[ab_1 V_{\max} + (a-1) b_2 V_{\max}^3 \right] R_{\mathrm{MW}}^2,$$

where the first term in the right hand is much smaller than the second term and can be omitted. Then we have

$$E \approx (a-1) b_2 V_{\max}^3 R_{\mathrm{MW}}^2. \quad \text{(A1)}$$

Taking logarithms of both sides of eq. (A1), we have

$$\log E = A + 3\log V_{\max} + 2\log R_{\mathrm{MW}}. \quad \text{(A2)}$$

Taking WNP for example, based on the Joint Typhoon Warning Center (JTWC) best track data of TCs over the WNP during 2001–2010, we obtained $V_{\max}$ and R_{MW} data with a sample size of 8096. Analysis on the data shows that the median of R_{MW} is 46.0 km and the interquartile range is 37.0 km, while the median of $V_{\max}$ is 120.4 km h^{-1} and the interquartile range is 101.9 km h^{-1} (Figure A1). That is to say, both the average and variability of $V_{\max}$ are much larger than R_{MW}. Therefore, the term of $V_{\max}$ is much larger than the term of R_{MW} in eq. (A2).

Moreover, the linear correlation coefficient of $V_{\max}$ and R_{MW} is about –0.63, while the order correlation coefficient is about –0.69, both indicate close relationship between the two variables. Apply a polynomial regression of R_{MW} on $V_{\max}$, we have

$$\hat{R}_{\mathrm{MW}} = 105.0 - 1.311 \times V_{\max} + 0.006 \times V_{\max}^2. \quad \text{(A3)}$$

Both the regression equation and its coefficient are significant at 99.9% confidence, and R^2=0.46. The probability distribution of the regression residuals of R_{MW} is shown in Figure A2. Obviously, although the probability distribution has long tails, its main part is narrow, with the interquartile range about 19.3 km. That is to say, about 50% of the residuals are on [–11.3, 8.0], and about 70% are on [–15.5, 16.3]. This further suggests that the variation of most residuals of R_{MW} is not large. Moreover, the geographic distribution of the residuals of R_{MW} (Figure A3) also indicates the residuals of R_{MW} are quite homogeneous in most part of the WNP, with a range of ±10 km. According to eqs. (A2) and (A3), the contribution of residuals of R_{MW} to E is smaller than the contribution of $V_{\max}$.

In summary, although it may introduce uncertainties as defining AEI without considering the TC sizes, it is reasonable and acceptable to use AEI as an index of TC's energy change for the purpose of this study as there are insufficient TC size data.

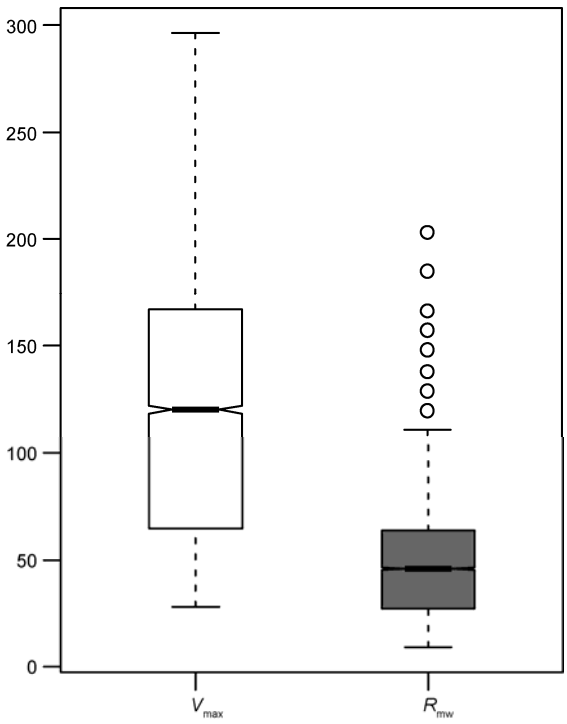

Figure A1 The box-and-whisker plot for the maximum sustained wind $V_{\max}$ (km h^{-1}) and its corresponding radius R_{MW} (km).

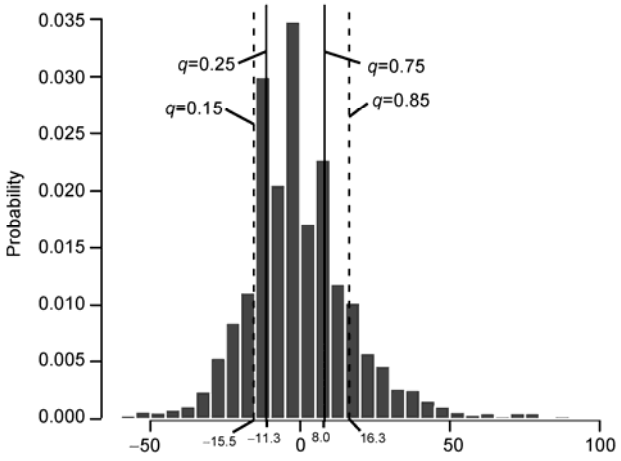

Figure A2 The probability distribution and quantiles for the regression residuals of R_{MW} (km).

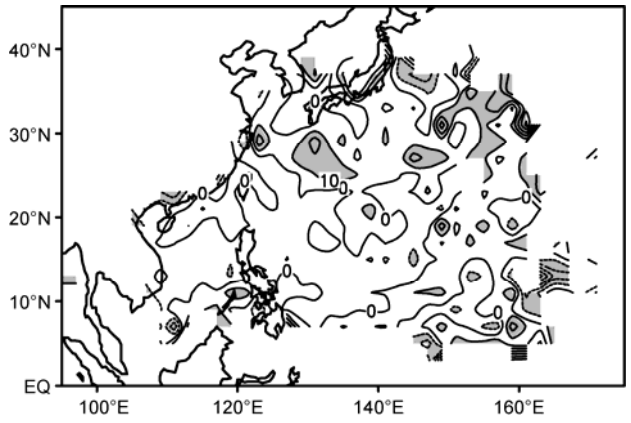

Figure A3 The geographic distribution of the regression residuals of R_{MW} (km).

We sincerely thank two anonymous reviewers for their insightful comments on an earlier version of this paper, which helped to include the impacts of

tropical cyclone sizes and improve the presentation of this study. This work was supported jointly by the National Basic Research Program of China (Grant Nos. 2010CB950403, 2012CB956003 and 2012CB417203), and the National Natural Science Foundation of China (Grant Nos. 40925015 and 41075071).

1 Ramage C S. Monsoon Meteorology. New York and London: Academic Press, 1971. 296
2 Halley E. An historical account of the trade winds and monsoons observable in the seas between and near the tropics with an attempt to assign the physical cause of the said wind. Phil Trans Roy Soc Lond, 1686, 16: 153–168
3 Webster P J, Chou L, Lau K M. Mechanisms effecting the state, evolution and transition of the planetary scale monsoon. Pageoph, 1977, 115: 1463–1491
4 Wu G, Liu Y. Summertime quadruplet heating pattern in the subtropics and the associated atmospheric circulation. Geophys Res Lett, 2003, 30: 1201
5 Liu Y, Wu G, Ren R. Relationship between the subtropical anticyclone and diabatic heating. J Clim, 2004, 17: 682–698
6 Wu G, Liu Y, Yu J, et al. Modulation of land-sea distribution on air-sea interaction and formation of subtropical anticyclones (in Chinese). Chin J Atmos Sci, 2008, 32: 720–740
7 Guan Y. The influence of air-sea interaction on the formation of monsoon onset vortex over BOB and the Asian monsoon onset. Dissertation for the Doctoral Degree. Beijing: Graduate University of Chinese Academy of Sciences, 2010. 115
8 Gray W M. Hurricanes: Their formation, structure and likely role in the tropical circulation. In: Meteorology over the Tropical Oceans. London: Royal Meteorological Society, 1979. 115–218
9 Lighthill J, Holland G, Gray W, et al. Global climate change and tropical cyclones. Bull Amer Meteor Soc, 1994, 75: 2147–2157
10 Li C. El Niño and western Pacific tropical cyclone activity. Chin Sci Bull, 1985, 30: 1087–1089
11 Gray W M. Atlantic seasonal hurricane frequency. Part I. El Niño and 30 mb Quasi-Biennial Oscillation influences. Mon Weather Rev, 1984, 112: 1649–1668
12 Wu G, Lau N C. A GCM Simulation of the relationship between tropical-storm formation and ENSO. Mon Weather Rev, 1992, 120: 958–997
13 Wang B, Chan J C L. How strong ENSO events affect tropical storm activity over the western North Pacific. J Clim, 2002, 15: 1643–1658
14 Chen L, Ding Y. An Introduction to West Pacific Typhoons (in Chinese). Beijing: Science Press, 1979. 491
15 Ding Y, Reiter E R. Large-scale circulation conditions affecting the typhoon formation over the west Pacific. Acta Oceanol Sin, 1983, 3: 327–338.
16 Jiang L, Ying M. Analysis of anomalous frequency of tropical cyclone in East China (in Chinese). J Appl Meteor Sci, 2002, 13: 88–95
17 Liu G, Sun S, Zhang Q, et al. Characteristics of the intraseasonal oscillation of intertropical convergence zone and its influence on the periodical tropical cyclogenesis (in Chinese). Chin J Atmos Sci, 2009, 33: 879–889
18 Gao J, Zhang X, Jiang Z, et al. Anomalous western North Pacific monsoon trough and tropical cyclone activities (in Chinese). Acta Oceanol Sin, 2008, 30: 35–47
19 Harr P A, Elsberry R L. Large-scale circulation variability over the tropical western North Pacific. Part I: Spatial patterns and tropical cyclone characteristics. Mon Weather Rev, 1995, 123: 1125–1246
20 Chan J C L, Shi J E, Lam C M. Seasonal forecasting of tropical cyclone activity over the western North Pacific and the South China Sea. Wea Forecasting, 1998, 13: 997–1004
21 Li Z. The onset of equatorial westerlies and tropical cyclone activity over the western North Pacific (in Chinese). In: Proceeding of the Conference on Tropical Circulation and Systems. Beijing: China Ocean Press, 1982. 129–139
22 Holland G J. Global guide to tropical cyclone forecasting, WMO/TD-No. 560, Report No. TCP-31. Geneva, Switzerland: WMO, 1993.
23 Clement A C, Seager R, Murtugudde R. Why are there tropical warm pools? J Clim, 2005, 18: 5294–5311
24 Zhou Z, Jin X, Wang L, et al. Two closures of the Indonesian seaway and its relationship to the formation and evolution of the western Pacific warm pool (in Chinese). Mar Geol Quat Geol, 2004, 24: 7–14
25 Peixoto J P, Oort A H, Physics of Climate. New York: American Institute of Physics, 1992. 520
26 Chen G, Huang R. Research on climatological problems of tropical cyclone and typhoon activity in western North Pacific (in Chinese). Adv Earth Sci, 2006, 21: 610–616
27 Huang R, Chen G. Research on interannual variations of tracks of tropical cyclones over Northwest Pacific and their physical mechanism (in Chinese). Acta Meteorol Sin, 2007, 65: 485–496
28 Ren F, Wang X, Dong W, et al. Changes in the first-landfall and last-landfall tropical cyclones in China (in Chinese). Adv Clim Change Res, 2007, 3: 224–228
29 Xie J. Analysis and prediction on the earliest and latest tropical cyclones landfalling on Guangdong Province (in Chinese). Mar Forecasts, 1999, 16: 62–68
30 Emanuel K. An air-sea interaction theory for tropical cyclones. Part I. Steady-state maintenance. J Atmos Sci, 1986, 42: 1062–1071
31 Bister M, Emanuel K A. Dissipative heating and hurricane intensity. Meteorol Atmos Phys, 1998, 50: 233–240
32 Emanuel K. Increasing destructiveness of tropical cyclones over the past 30 years. Nature, 2005, 436: 687–688
33 Webster P J, Holland G J, Curry J A. Changes in tropical cyclone number, duration, and intensity in a warming environment. Science, 2005, 309: 1844–1846
34 Emanuel K A. Contribution of tropical cyclones to meridional heat transport by the oceans. J Geophys Res, 2001, 106: 14771–14781
35 Korty R L, Emanuel K A, Scott J R. Tropical cyclone-induced upper-ocean mixing and climate: Application to equable climates. J Clim, 2007, 21: 638–654
36 Pasquero C, Emanuel K A. Tropical cyclones and transient upper-ocean warming. J Clim, 2008, 21: 149–162
37 Gray W M, Landsea C W, Mielke Jr P W, et al. Predicting Atlantic seasonal hurricane activity 6–11 months in advance. Wea Forecasting, 1992, 7: 440–455
38 Bell G D, Halpert M S, Schnell R C, et al. Climate assessment for 1999. Bull Amer Meteor Soc, 2000, 81: s1–s50
39 Kwon H J, Lee W J, Won S H, et al. Statistical ensemble prediction of the tropical cyclone activity over the western North Pacific. Geophys Res Lett, 2007, 34: L24805
40 Wu L, Wang B, Braun S A. Implications of tropical cyclone power dissipation index. Int J Climatol, 2008, 28: 727–731
41 Knapp K R, Kruk M C, Levinson D H, et al. The International Best Track Archive for Climate Stewardship (IBTrACS): Unifying tropical cyclone best track data. Bull Amer Meteor Soc, 2010, 91: 363–376
42 Standardization Administration of P. R. China. Grade of Tropical Cyclones. GB/T 19201–2006, 2006
43 Kanley E, Kanamitsu M, Kistler R, et al. The NCEP/NCAR 40-year reanalysis project. Bull Amer Meteor Soc, 1996, 77: 437–471
44 Yanai M, Esbensen S, Chu J H. Determination of bulk properties of tropical cloud clusters from large-scale heat and moisture budgets. J Atmos Sci, 1973, 30: 611–627
45 Luo H, Yanai M. The Large-scale circulation and heat sources over the Tibetan Plateau and surrounding areas during the early summer of 1979. Part II: Heat and moisture budgets. Mon Weather Rev, 1984, 112: 966–989
46 Yanai M, Tomita T. Seasonal and interannual variability of atmospheric heat sources and moisture sinks as determined from NCEP-NCAR reanalysis. J Clim, 1998, 11: 463–482
47 Emanuel K. Sensitivity of tropical cyclones to surface exchange coefficients and a revised steady-state model incorporating eye dynam-

ics. J Atmos Sci, 1995, 52: 3969–3976
48 Yuan J, Wang D, Wan Q, et al. A 28-year climateological analysis of size parameters for northwestern Pacific tropical cyclones. Adv Atmos Sci, 2007, 24: 24–34
49 Weatherford C L, Gray W M. Typhoon structure as revealed by aircraft reconnaissance. Part I: Data analysis and climatology. Mon Weather Rev, 1988, 116: 1032–1043
50 Mallen K J, Montgomery M T, Wang B. Reexaming the near-core radial structure of the tropical cyclone primary circulation: Implications for votex resiliency. J Atmos Sci, 2005, 62: 408–425
51 Firerson D M W, Held I M, Zurita-Gotor P. A Gray-radiation aquaplanet moist GCM. Part I: Static stability and eddy scale. J Atmos Sci, 2006, 63: 2548–2566
52 Liu Y, Guo L, Wu G, et al. Sensitivity of ITCZ configuration to cumulus convective parameterizations on an aqua planet. Clim Dyn, 2010, 34: 223–240
53 Maloney E D, Sobel A H, Hannah W M. Intraseasonal variability in an aquaplanet general circulation model. J Adv Model Earth Syst, 2010, 2: 24
54 Rodgers E B, Adler R F, Pierce H F. Contribution of tropical cyclones to the North Pacific climatological rainfall as observed from Satellites. J Appl Meteorol, 2000, 39: 1658–1678
55 Rodgers E B, Adler R F, Pierce H F. Contribution of tropical cyclones to the North Atlantic climatological rainfall as observed from Satellites. J Appl Meteorol, 2001, 40: 1785–1800
56 Wei Q, Ren F, Zhang Q, et al. Climatological characteristics of tropical cyclone precipitation over western North Pacific (in Chinese). J Trop Meteorol, 2010, 26: 293–300
57 Wu G, Liu Y. Thermal adaptation, overshooting, dispersion, and subtropical anticyclone. Part I. Thermal adaptation and overshooting (in Chinese). Chin J Atmos Sci, 2000, 24: 433–446
58 Liu Y, Wu G, Yu R, et al. Thermal adaptation, overshooting, dispersion, and subtropical anticyclone. Part II. Horizontal inhomogeneous heating and energy dispersion (in Chinese). Chin J Atmos Sci, 2001, 25: 317–328
59 Gill A E. Some simple solutions for heat-induced tropical circulation. Quart J R Met Soc, 1980, 106: 447–462
60 Li J. Zeng Q. A new monsoon index and the geographical distribution of the global monsoons. Adv Atmos Sci, 2003, 20: 299–302
61 Webster P J, Chang H R. Equatorial energy accumulation and emanation regions: impacts of a zonally varying basic state. J Atmos Sci, 1988, 45: 803–829
62 Gray W M, Landsea C W. African rainfall as a precursor of hurricane-related destruction on the U.S. East Coast. Bull Amer Meteor Soc, 1992, 73: 1352–1364
63 Wu G, Zhang Y. Tibetan Plateau rorcing and monsoon onset in South Asia and Southern China Sea. Mon Weather Rev, 1998, 126: 913–927
64 Emanuel K. Tropical cyclones. Ann Rev Earth Planet Sci, 2003, 31: 75–104